A MATHEMATICAL MODEL OF THE TOTAL CURRENT DYNAMICS IN HAIR CELLS

V. V. Alexandrov[1], A. Almanza[2], N. V. Kulikovskaya[1], R. Vega[2], T. B. Alexandrova[1], N. E. Shulenina[1], A. Limón[2], and E. Soto[2]

The participation of hair cells in the analysis of sensory scene and their sensory segregation capabilities are not yet fully understood. Subtypes of hair cells have been defined from a morphological point of view. Important differences in the expression of ionic currents between hair cells have been reported, but up to now, a full picture of the influence of hair cell diversity on the vestibular sensory coding is lacking. The total ionic current and voltage responses to current injection were studied in isolated hair cells from the axolotl (*Ambystoma tigrinum*) utricle and semicircular canals. In both endorgans the total current of the hair cells was dominated by an outward-going current that partially inactivates. The cells from the utricle have a slower current kinetics than those from the semicircular canals. The maximal conductance, activation time constant, voltage dependence of activation, inactivation time constant, and voltage dependence of inactivation are considered as characteristics of the total current. A Hodgkin–Huxley type model of the total current in the hair cell was developed. The data obtained from experimental measurements in form of current-to-voltage dependence were used for the definition of the parameters for the model. Model results showed that the hair cell response can reasonably be modeled using the total outward ionic current. Our results demonstrate that the hair cell responses are predominant due to the outward ionic currents. The variability in the expression of voltage dependent ionic currents among hair cells endows the vestibular system endorgans with the capability of feature extraction from the sensory stimuli.

1. Introduction. Hair cells from the inner ear form part of an epithelium that separates two fluids with different ionic compositions. The hair cell basolateral membrane faces the perilymph (with low K^+ and high Na^+ ionic concentrations), whereas the apical side of a cell is in contact with the endolymph (with high K^+ and low Na^+ composition). These peculiar conditions imply that the generation of the membrane potential would be complex. Nonhomogeneous currents arise in different regions of the cell membrane, depending on the local permeabilities and on the ionic concentrations in the surrounding fluid (Figure 1).

The hair cell membrane potential (when cilia are not bent) results from the interplay of the apical and basolateral permeabilities. The apical one (a nonspecific cationic permeability) drives the membrane potential close to zero. *In vivo*, the current through the apical membrane is generated mainly by K^+ ions (due to the high K^+ endolymphatic concentration, its resting potential is close to zero mV). The basolateral permeability (mainly, due to K^+ ions) drives the membrane potential to the K^+ equilibrium potential which is close to -85 mV. The resting membrane potential may be determined by the Goldman–Hodgkin–Katz equation [32]:

$$V_{\mathrm{rest}} = \frac{RT}{F} \ln \frac{P_{\mathrm{transd}}[\mathrm{K}]_{\mathrm{e}} + P_{\mathrm{K,p}}[\mathrm{K}]_{\mathrm{p}} + P_{\mathrm{Na,p}}[\mathrm{Na}]_{\mathrm{p}}}{P_{\mathrm{Na,p}}[\mathrm{Na}]_{\mathrm{i}} + (P_{\mathrm{transd}} + P_{\mathrm{K,p}})[\mathrm{K}]_{\mathrm{i}}}$$

Here R, T, and F have their usual meaning as the gas constant, absolute temperature, and the Faraday constant, respectively; P_{transd} is the mechanoelectrical transducer permeability to K^+ ions; $P_{\mathrm{K},p}$ is the total potassium permeability of the basolateral membrane; $P_{\mathrm{Na},p}$ is the total Na^+ permeability of the basolateral membrane.

As a consequence of the above, the basal membrane potential will lie between 0 and -85 mV, depending on the relative values of the apical and basal permeabilities. It is clear that the current will flow through the apical and basolateral membranes (from the endolymph to the inside of the cell and from the cell to the perilymph). The open probability of the mechanotransducer channels controls the current flow. If the open probability is low, the current is negligible and the cell potential is close to the equilibrium potential of the basal membrane (tends to -85 mV). If the open probability of the mechanotransducer channels is large, the hair cell potential tends to the equilibrium potential of the apical membrane (i.e., to zero).

[1] Faculty of Mechanics and Mathematics, Moscow State University, Moscow, 119899, Russian Federation, e-mail: valex@moids.math.msu.ru; nvkpostb@mtu-net.ru; i_nelly@hotmail.com
[2] Instituto de Fisiología, Universidad Autónoma de Puebla, Apartado Postal 406, Puebla, Pue. 72000, México, e-mail: esoto@siu.buap.mx

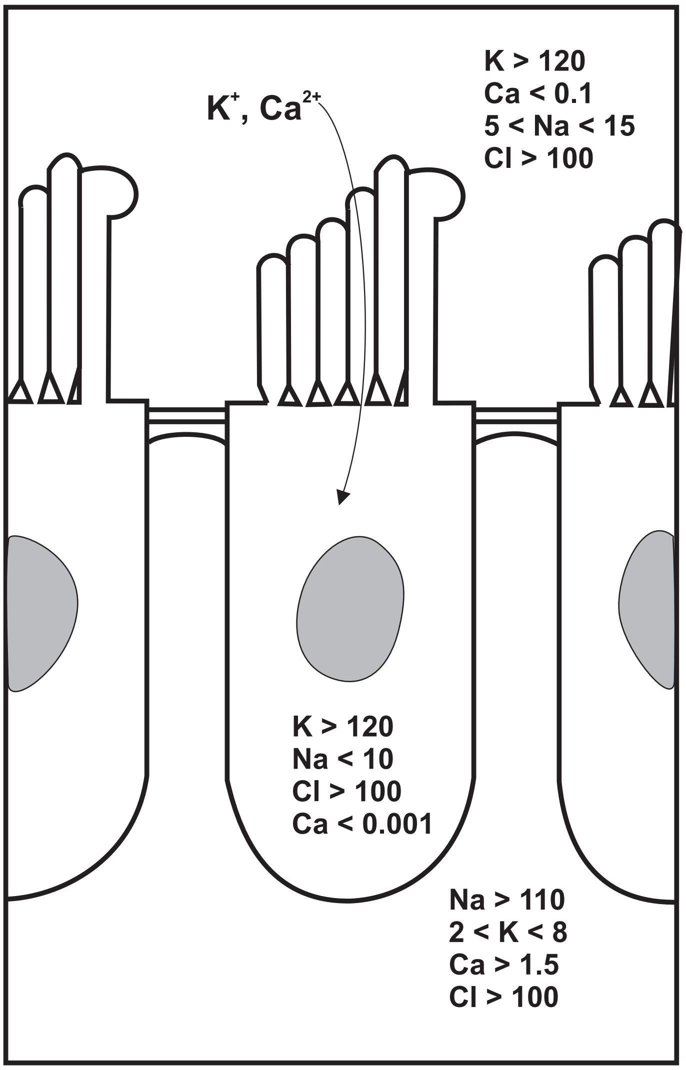

Fig. 1. Scheme summarizes the hair cell ionic media. Data on ionic compositions of the endo- and perilymph are given as concentration for each ion (in mM/L). Due to the very peculiar endolymph ionic composition, the mechanoelectrical transducer current is carried mainly by K^+ ions and, in a very low proportion, by Ca^{2+} ions. Depolarization of a hair cell by the transducer current determines the activation of voltage-dependent ionic currents in the basolateral surface of the hair cells, leading to an important outflow of K^+ ions, which, in this case, constitutes an outward current that repolarizes the cell

The voltage-activated conductances of the basolateral membrane of the hair cells varies (depending on the animal species) in the region of the inner ear from which the cells originate and at the developmental stage of the animal [7, 20]. However, the hair cells share some characteristic ionic currents and, in all the cells studied up to now, the potassium currents dominate the basolateral membrane response [16, 18].

Although there is a profound knowledge of the voltage-dependent conductance in the vestibular hair cells, some important aspects of their response remain unsolved up to now. The aim of our work is to create a complete model of the vestibular endorgan function. This model may incorporate at least six components: a mechanical coupling mechanism, a mechanoelectrical transducer, a hair cell receptor potential, a neurotransmitter release component, a postsynaptic response mechanism, and a spike encoder mechanism (Figure 2). Such a model, if studied in every detail, could have an extreme complexity and be impossible to deal with. That is why we have decided to create a synthetic model that would allow us to integrate the basic processes leading to the sensory coding of vestibular information.

In this work, a simplified model for the receptor potential generation in hair cells is discussed (Figure 3). The model is based on the analysis of the total ionic current and the voltage responses registered from the

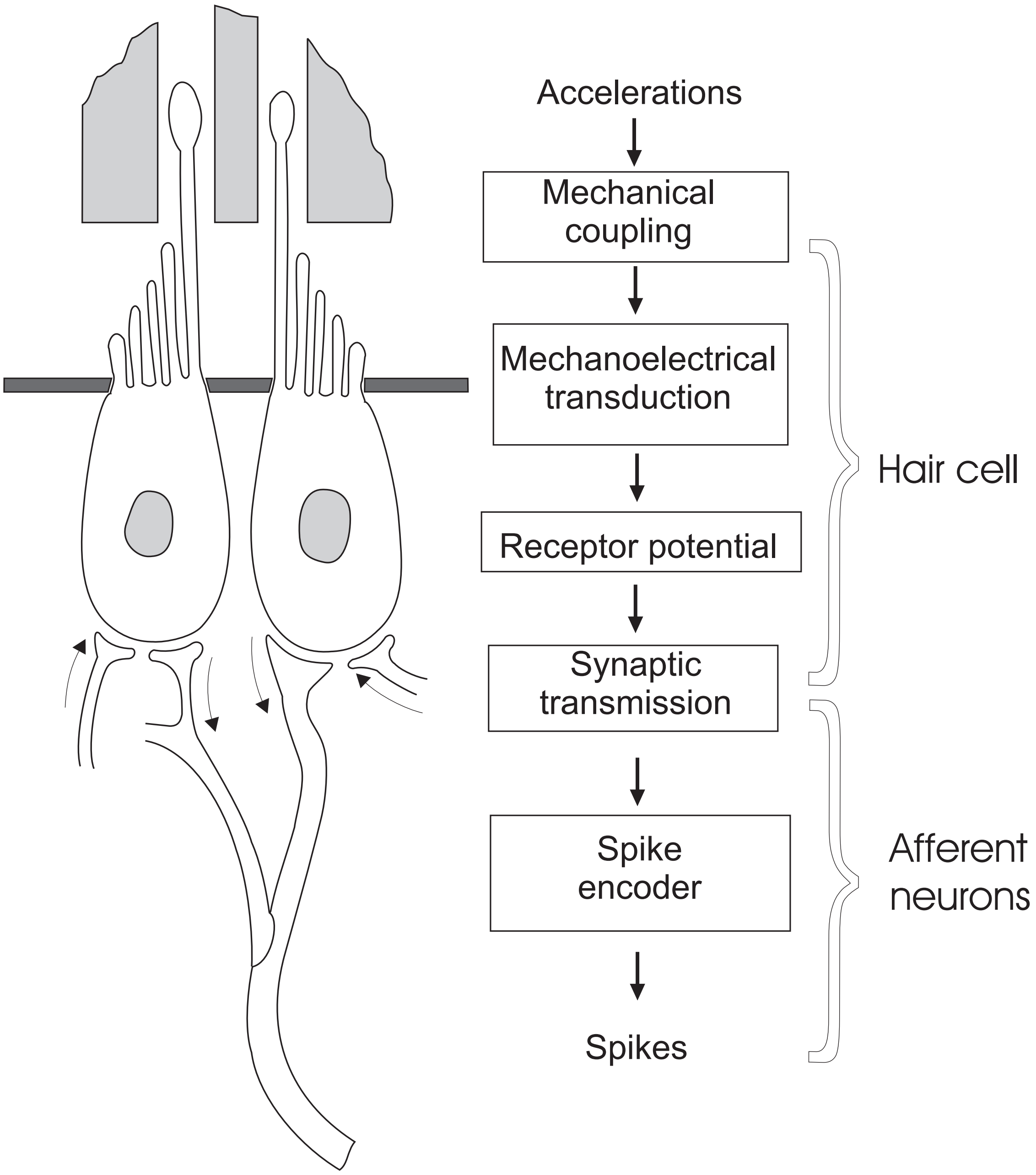

Fig. 2. Scheme of the series of events participating in the sensory coding in the vestibular endorgans. The input to the system is in the form of accelerations. The mechanical coupling determines the type of effective stimuli for the system (angular or linear accelerations). The hair cell receptor potential is the object of this work. The synaptic transmission and the spike encoder mechanism will be dealt with in future works

semicircular canal and the utricle hair cells isolated from the axolotl (*Ambystoma tigrinum*) inner ear.

2. Experimental methods. Our experiments were carried out with wild larval axolotls (*Ambystoma tigrinum*, 30 to 60 g in weight) as reported previously [29, 30]. The animals were anesthetized by immersion in 3-aminobenzoic acid ethyl ester (0.1 % in proportion to water) and were subsequently decapitated. The otic capsule was opened ventrally and the inner ear structures were identified.

Hair cell voltage clamp recordings. The semicircular canals or the utricle were dissected from the inner ear, and the hair cells were enzymatically dissociated. To accomplish this, the tissue pieces were incubated with collagenase (0.1 mg/ml) during 7 min at 30° C in normal external solution of the following composition (in mM): NaCl 111; KCl 5; HEPES 5; $MgCl_2$ 1; $CaCl_2$ 1.8; glucose 10; osmolarity 240 mOsm/Kg and the pH adjusted with NaOH to 7.4. The tissue sections were then transferred to the external Ringer solution without Ca^{2+}

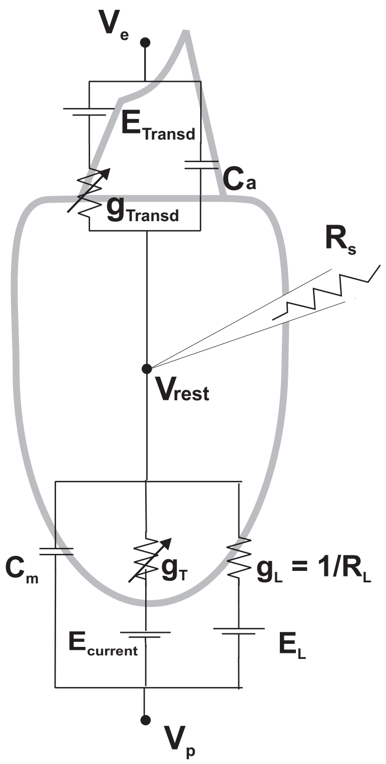

Fig. 3. Scheme of the equivalent circuit of the simplified model of the hair cell ionic currents. The variable resistances represent the mechanogated ionic channels for the transducer current (g_{Transd}) and the voltage-sensitive ionic channels for the basolateral membrane (g_{T}). The leakage conductance is represented as a invariable resistance (g_{L}). The transducer current equilibrium potential (E_{Transd}) is thought of to be close to zero, since the channels are nonselective to cations. The basal membrane equilibrium potential is close to the equilibrium potential for K^+ ($E_{\mathrm{current}} \approx E_{\mathrm{K}}$), since this is the most permeable ion in the basolateral membrane. The leakage permeability is nonselective and its equilibrium potential is thus close to zero (E_{L}). The capacitance is distributed between the apical (C_{a}) and basolateral (C_{m}) membranes. V_{p} is the perilymphatic potential, V_{e} is the endolymphatic potential, V_{rest} is the resting potential

and Mg^{2+} and added with trypsin (1 mg/ml). After 10 min at 30° C, they were transferred to the normal external Ringer solution without Ca^{2+} and Mg^{2+} added with albumin (1 mg/ml) at 4° C. After 5 min, the tissue sections were placed in the recording chamber located in the stage of an inverted microscope (Nikon, Diaphot) and the hair cells were isolated by gently scratching with two glass bars.

Once the cells settled down, the recording chamber was continuously perfused with the normal external solution at a constant rate of 0.5 ml/min, using a peristaltic pump (LKB, Microperpex). The experiments were carried out at room temperature (22 – 25° C). The isolated cells were recorded with the use of the patch-clamp technique in the whole cell voltage-clamp configuration according to the method described in [9]. Patch clamp pipettes were fabricated from borosilicate (hard) glass capillary tubing of outside diameter 1.2 mm (WPI), using a horizontal Flaming Brown micropipette puller (P80/PC Sutter Instruments). The patch pipettes used for the whole-cell recording had resistances of 2 – 4 MΩ when filled with the intracellular solution (in mM/L): NaCl 10; KCl 100; EGTA 2 (K^+ salt); HEPES 10; $\mathrm{MgCl_2}$ 2; $\mathrm{CaCl_2}$ 0.134; adjusted with KOH to pH 7.2; osmolarity was 240 mOsm/Kg as measured using a vapor pressure osmometer (Wescor 5500).

Data were recorded with an Axopatch 200B amplifier (Axon Instruments) whose output was led to a 12-bit digital-analog converter (Digidata 1200) controlled by the pClamp 8.0 software (Axon Instruments).

Data were low-pass filtered at 2 KHz and sampled at 100 μs intervals. Voltages were not corrected for either liquid junction potential or uncompensated series resistance. The correction for the leakage current was made when stated in the text.

Voltage and current clamp procedures. The electrode resistance was directly measured in the saline solution by applying a constant voltage pulse and measuring the resultant current: $R_e = V/I$. In our experiments, the electrode resistance was always between 2 and 4 MΩ.

Once the cell was touched with the electrode, the capacitive transients were nulled and time was allowed for the seal resistance (R_{seal}) between the cell and the electrode to grow above 1 GΩ (commonly, no negative pressure was needed for the seal resistance to grow, but in some experiments a slight negative pressure should be applied to establish the gigaohm seal).

Once the gigaohm seal was established, the cell membrane was ruptured and the system went into the whole cell patch clamp configuration; the access resistance, membrane resistance, membrane time constant, capacitance, and holding current were calculated online by the pClamp 8 software (see [2]). However, a -10 mV pulse relative to $V_{\text{hold}} = -70$ mV was registered in all the cells we studied. The current thus produced was used to measure (offline) the seal resistance, the capacitance and the membrane time constant (τ), from which the series resistance (R_s) of recording was calculated, since $\tau = R_s \times C$. Once the passive properties were recorded, the capacitive transient and the series resistance were electronically compensated. The series resistance was compensated up to 80 % with 10 ms time lag [1].

The voltage-activated ionic currents were produced by using various protocols. The total ionic current was activated using a double-pulse voltage clamp protocol in which V_{hold} was -85 mV and a series of test pulses of duration 800 ms ranging from -130 to 50 mV (V_{test1}) in steps of 10 mV were followed by a 200 ms pulse to 20 mV (V_{test2}). The first pulse series allowed measuring the activation parameters of the current and the inactivation time constant. The second pulse series allowed defining the steady-state inactivation of the total current.

For the current clamp experiments, the cell membrane potential was set to -70 mV by current injection. A series of current pulses ranging from -0.5 to 0.5 nA in steps of 0.1 nA and with duration of 800 ms were applied with intervals of 5 s.

3. Data analysis. The data analysis was done taking in mind that experiments were focussed to identify the model parameters. Our work is based on the Hodgkin–Huxley model [8, 10–13]. The ionic cell current can be written down as

$$I = I_{\text{T}} + I_{\text{L}} \tag{1}$$

where $I_{\text{L}} = g_{\text{L}} \cdot V$ is the leakage current (its conductance is voltage-independent and its reverse potential is close to zero), I_{T} is the total current flowing through voltage-dependent ionic channels. The reverse potential E_{T} for I_{T} is in the range between -105 to -65 mV. The I_{T} can be described as

$$I_{\text{T}} = \bar{g}_{\text{T}} \cdot m^r \cdot (h_1 + h_2) \cdot (V - E_{\text{T}}) \tag{2}$$

where $\bar{g}_{\text{T}}$ is the maximal value of the conductance, m^r is the parameter that describes the activation process, h_1 and h_2 are the parameters that describe the inactivation process, and E_{T} is the equilibrium potential for the total current (in the hair cells, this last variable is very close to the K^+ equilibrium potential, i.e., $E_{\text{T}} \approx E_{\text{K}}$).

The time dependence of the parameters m, h_1, and h_2 can be described by the following system of first-order differential equations:

$$\begin{aligned} \tau_m(V)\,\frac{dm}{dt} + m &= m_{\text{st}}(V) \\ \tau_{h1}(V)\,\frac{dh_1}{dt} + h_1 &= q_1 h_{\text{st}}(V) = h_{1\text{st}}(V) \\ \tau_{h2}(V)\,\frac{dh_2}{dt} + h_2 &= q_2 h_{\text{st}}(V) = h_{2\text{st}}(V) \end{aligned} \tag{3}$$

Here q_1 and q_2 have their values between 0 and 1 and are the relative weights of the fast and slow inactivations, respectively. The voltage dependence of m, h_1, and h_2 are given by the functions m_{st}, $h_{1\text{st}}$, and $h_{2\text{st}}$. These functions can be described as the following first-order Boltzmann functions

$$m_{\text{st}}(V) = m_{\min} + \frac{1 - m_{\min}}{1 + \exp\left(-\frac{V - V_{\text{ac}}}{S_{\text{ac}}}\right)}, \quad h_{\text{st}}(V) = h_{\min} + \frac{1 - h_{\min}}{1 + \exp\left(\frac{V - V_h}{S_h}\right)} \tag{4}$$

The activation and inactivation time constants, in the general case, are also functions of voltage (V) and can be described as

$$\tau_m(V) = \tau_{\min} + \frac{\tau_{\max} - \tau_{\min}}{1 + \exp\left(\frac{V - V_\tau}{S_\tau}\right)}, \quad \tau_{h1}(V) = k_{h1} \cdot V + b_{h1}, \quad \tau_{h2}(V) = k_{h2} \cdot V + b_{h2} \tag{5}$$

According to the results of our computations confirmed by the data from the literature, we found that the inactivation time constants τ_{h1} and τ_{h2} depend on the voltage V weakly. It is quite enough to approximate τ_{h1}

and τ_{h2} by straight lines with small slope angles with the parameters k_{h1}, k_{h2}, b_{h1}, and b_{h2}. The numerical parameters entering into (4) and (5) should be determined for each cell during the experimental recording of ionic currents under voltage clamp conditions as described below.

The cell recordings and model simulations presented in this work were analyzed using the Clampfit 8.0 software (Axon Instruments). The data processing for each cell recording was as follows.

1. Determination of the passive membrane properties C_m, V_{rest}, and R_m is fulfilled in the experiment online for each cell.

2. Determination of the current time constants: τ_m, τ_{h1}, and τ_{h2}. Each time constant can be calculated in different recordings according to the sampling rate used and to the particular experimental conditions that permit a correct time definition of its value. Values of these time constants can be obtained with the use of approximate formulas for the ionic currents as known time functions with unknown parameters.

For the voltage clamp protocol when

$$V(t) = \begin{cases} V_{\text{hold}}, & t \leqslant t_0 \\ V^i_{\text{test1}}, & t > t_0, \quad i = 1, \dots, N \end{cases}$$

the initial conditions for equation (3) are

$$m(t_0) = m_{\text{st}}(V_{\text{hold}}), \quad h_1(t_0) = h_{1\text{st}}(V_{\text{hold}}), \quad h_2(t_0) = h_{2\text{st}}(V_{\text{hold}}) \tag{6}$$

Solving equation (3) with these initial conditions, we obtain

$$\begin{aligned} m(t) &= \left[m_{\text{st}}(V_{\text{hold}}) - m_{\text{st}}(V^i_{\text{test1}})\right] \cdot \exp\left(\frac{-(t-t_0)}{\tau_m(V^i_{\text{test1}})}\right) + m_{\text{st}}(V^i_{\text{test1}}) \\ h_1(t) &= \left[h_{1\text{st}}(V_{\text{hold}}) - h_{1\text{st}}(V^i_{\text{test1}})\right] \cdot \exp\left(\frac{-(t-t_0)}{\tau_{h1}(V^i_{\text{test1}})}\right) + h_{1\text{st}}(V^i_{\text{test1}}) \\ h_2(t) &= \left[h_{2\text{st}}(V_{\text{hold}}) - h_{2\text{st}}(V^i_{\text{test1}})\right] \cdot \exp\left(\frac{-(t-t_0)}{\tau_{h2}(V^i_{\text{test1}})}\right) + h_{2\text{st}}(V^i_{\text{test1}}) \end{aligned} \tag{7}$$

Substituting (7) into (2) and taking into account that $h_{1\text{st}} + h_{2\text{st}} = (q_1 + q_2) \cdot h_{\text{st}}$, we get

$$\begin{aligned} I^i_{\text{T}}(t) = {} & \bar{g}_{\text{T}} \cdot \left(V^i_{\text{test1}} - E_{\text{T}}\right) \cdot m^r_{\text{st}}\left(V^i_{\text{test1}}\right) \cdot (q_1 + q_2) \cdot h_{\text{st}}\left(V^i_{\text{test1}}\right) \\ & \times \left[1 + \frac{m_{\text{st}}(V_{\text{hold}}) - m_{\text{st}}(V^i_{\text{test1}})}{m_{\text{st}}(V^i_{\text{test1}})} \exp\frac{-(t-t_0)}{\tau_m(V^i_{\text{test1}})}\right]^r \\ & \times \left[1 + \frac{h_{1\text{st}}(V_{\text{hold}}) - h_{1\text{st}}(V^i_{\text{test1}})}{(q_1+q_2)\cdot h_{\text{st}}(V^i_{\text{test1}})} \exp\frac{-(t-t_0)}{\tau_{h1}(V^i_{\text{test1}})} + \frac{h_{2\text{st}}(V_{\text{hold}}) - h_{2\text{st}}(V^i_{\text{test1}})}{(q_1+q_2)\cdot h_{\text{st}}(V^i_{\text{test1}})} \exp\frac{-(t-t_0)}{\tau_{h2}(V^i_{\text{test1}})}\right] \end{aligned} \tag{8}$$

As a result, we obtain the expression

$$I^i_{\text{T}}(t) = \left(1 - P^i_6 \cdot \exp\frac{-(t-t_0)}{P^i_1}\right)^r \cdot \left(1 + P^i_4 \cdot \exp\frac{-(t-t_0)}{P^i_2} + P^i_5 \cdot \exp\frac{-(t-t_0)}{P^i_3}\right) \cdot P^i_7 \tag{9}$$

The values of the parameters $P^i_1, \dots, P^i_7$ for the ith current trace can be obtained approximately as follows:

$$\begin{aligned} P^i_1 &= \tau_m(V^i_{\text{test1}}) \\ P^i_2 &= \tau_{h1}(V^i_{\text{test1}}) \\ P^i_3 &= \tau_{h2}(V^i_{\text{test1}}) \\ P^i_4 &= q_1 \frac{h_{st}(V_{\text{hold}}) - h_{\text{st}}(V^i_{\text{test1}})}{(q_1+q_2)\cdot h_{\text{st}}(V^i_{\text{test1}})} \\ P^i_5 &= q_2 \frac{h_{\text{st}}(V_{\text{hold}}) - h_{\text{st}}(V^i_{\text{test1}})}{(q_1+q_2)\cdot h_{\text{st}}(V^i_{\text{test1}})} \\ P^i_6 &= -\frac{m_{\text{st}}(V_{\text{hold}}) - m_{\text{st}}(V^i_{\text{test1}})}{m_{\text{st}}(V^i_{\text{test1}})} \\ P^i_7 &= \bar{g}_{\text{T}} \cdot \left(V^i_{\text{test1}} - E_{\text{T}}\right) \cdot m^r_{\text{st}}\left(V^i_{\text{test1}}\right) \cdot (q_1 + q_2) \cdot h_{\text{st}}\left(V^i_{\text{test1}}\right) \end{aligned} \tag{10}$$

Note that parameters P_1^i, P_2^i, and P_3^i are of prime importance. From the above, we can calculate the numerical parameters that appear in (4) and (5).

3. Definition of the parameters for the activation $m_{\rm st}$ and inactivation $h_{1\rm st} + h_{2\rm st} = (q_1 + q_2) \cdot h_{\rm st}$ of the total current. To accomplish this, the experimental measurements of total current (1) are plotted as a function of the command voltage for three typical states: the peak current produced by $V_{\rm test1}$, the peak of the transient current produced by $V_{\rm test2}$, and the mean steady-state current values produced by $V_{\rm test1}$. These plots present experimental raw data, which are the sum of the total ionic current $I_{\rm T}$ and the leakage current $I_{\rm L}$. Since the leakage current $I_{\rm L}(V)$ is known, we can separate the total current $I_{\rm T}$ out from raw data for I (see (1)).

Let us consider the following steps of our analysis of the total current.

a) The maximal current $\max I_{\rm T}(V^i_{\rm test1})$ is reached with different time intervals for the different command potentials (i). Thus, the peak current is determined by calculating the maximum of the current in a time interval. Let us assume that

$$\tau_m(V^i_{\rm test1}) \ll \tau_{h1}(V^i_{\rm test1}) < \tau_{h2}(V^i_{\rm test1}) \tag{11}$$

Hence, the maximal current can be written with high accuracy as

$$\max_t I_{\rm T}(V^i_{\rm test1}) = \bar{g}_{\rm T} \cdot (V^i_{\rm test1} - E_{\rm T}) \cdot m^r_{\rm st}(V^i_{\rm test1}) \cdot (q_1 + q_2) \cdot h_{\rm st}(V_{\rm hold}) \tag{12}$$

b) When the command potential passes on from $V_{\rm test1}$ to $V_{\rm test2}$, under assumption (11) the peak of the transient current will depend on $V^i_{\rm test1}$:

$$\max_t I^i_{\rm T}(V_{\rm test2}) = \bar{g}_{\rm T} \cdot (V_{\rm test2} - E_{\rm T}) \cdot m^r(V_{\rm test2}) \cdot (q_1 + q_2) \cdot h_{\rm st}(V^i_{\rm test1}) \tag{13}$$

c) For the mean steady-state current we have the relation

$$I_{\rm Tst}(V^i_{\rm test1}) = \lim_{t \to t_1} I^i_{\rm T}(t) = \bar{g}_{\rm T} \cdot (V^i_{\rm test1} - E_{\rm T}) \cdot m^r_{\rm st}(V^i_{\rm test1}) \cdot (q_1 + q_2) \cdot h_{\rm st}(V^i_{\rm test1}) \tag{14}$$

d) Then we can determine the reverse potential of the total current $E_{\rm T} \approx E_{\rm K}$ as the voltage for which

$$I_{\rm Tst}(V^i_{\rm test1}) = 0 \quad \text{i.e.} \quad I_{\rm Tst}(E_{\rm T}) = 0$$

e) The steady-state inactivation of the ionic current $h_{\rm st}(V)$ can be determined as usually from

$$h_{\rm st}(V^i_{\rm test1}) = \frac{\max\limits_t I^i_{\rm T}(V_{\rm test2}, t)}{\max\limits_i \max\limits_t I^i_{\rm T}(V_{\rm test2}, t)} \tag{15}$$

We can obtain a more precise estimate for $V > 0$ according to the formula

$$h_{\rm st}(V^i_{\rm test1}) = \frac{I_{\rm Tst}(V^i_{\rm test1})}{\max\limits_t I_{\rm T}(V^i_{\rm test1}, t)} \tag{16}$$

and can specify the estimates of inactivation parameters for (4) as a result of fitting (15) and (16) expressed in the form

$$h_{\rm st}(V) = P_8 + \frac{1 - P_8}{1 + \exp \frac{V + P_9}{P_{10}}} \tag{17}$$

Here $P_8 = \tilde{h}_{\rm min}$, $P_9 = -\tilde{V}_h$, and $P_{10} = \tilde{S}_h$, where the symbol $\tilde{}$ indicates estimates for the corresponding parameters.

f) The steady-state activation $m_{\rm st}$ can be calculated at two stages. We first construct the conductance-versus-voltage curves according to

$$F(V) = \frac{\max I_{\rm T}(V^i_{\rm test1}, t)}{V^i_{\rm test1} - E_{\rm T}} = \bar{g}_{\rm T} \cdot m^r(V^i_{\rm test1}) \cdot (q_1 + q_2) \cdot h_{\rm st}(V_{\rm hold}) \tag{18}$$

and, then, adjust the conductance curve by the Boltzmann function with four parameters

$$F(V) = P_{14} \cdot \left(P_{11} + \frac{1 - P_{11}}{1 + \exp \frac{-(V + P_{12})}{P_{13}}} \right)^r \tag{19}$$

Similarly to the previous step, we get estimates for activation parameters and maximal conductance as a result of fitting (18) in the form $F(V) = P_{14} \cdot m(V)^r$, where $P_{11} = \widetilde{m}_{\min}$, $P_{12} = -\widetilde{V}_{\rm ac}$, $P_{13} = \tilde{S}_{\rm ac}$, $P_{14} = \tilde{g}_{\rm T} \cdot \tilde{h}_{\rm st}(V_{\rm hold})$.

Assuming that $\max F(V)$ is reached when $V > 0$ and $m = 1$, we obtain

$$P_{14} = \tilde{g}_{\rm T} \cdot \tilde{h}_{\rm st}(V_{\rm hold}) \tag{20}$$

$$m_{\rm st}(V) = P_{11} + \frac{1 - P_{11}}{1 + \exp \frac{-(V+P_{12})}{P_{13}}} \tag{21}$$

where P_{11} is the part of conductance activated when $V < E_{\rm T}$. Since the value of $\tilde{h}_{\rm st}(V_{\rm hold})$ is known, from (17) we can write down:

$$\tilde{g}_{\rm T} = \frac{P_{14}}{\tilde{h}_{\rm st}(V_{\rm hold})} \tag{22}$$

We name $m(V)$ as a variable of activation and the expression $\mathrm{ac}(V) = m(V)^r$ as the curve of activation. We will use different symbols for variable m and $\mathrm{ac}(V)$ for analysis convenience of the experimental results.

The curve $\mathrm{ac}(V)$ can be adjusted using the Boltzmann function with the parameters $V_{\rm cur-ac}$, $S_{\rm cur-ac}$, and $\min_{\rm ac}$. When $r = 1$, the variable of activation coincides with the curve of activation.

The data represented in Figure 5 A, 6 A (average estimation) were obtained for $\mathrm{ac}(V)$.

Remark. Formula (18) for the conductance curve can be applied if the size of $E_{\rm T}$ is known. On the other hand, it is possible to calculate the *chord* conductance (the difference quotient of the current stationary value to the test potential). Therefore, formulas (19) – (22) can be used. One of these approaches can be chosen as the most reliable one for each particular case.

4. Experimental results. *Passive properties.* The passive properties of hair cells isolated from the semicircular canals and from the utricle were measured under various conditions; the data we obtained are summarized in Table I.

Table I. The passive membrane properties of axolotl hair cells

	R_m	C_m	$V_{\rm rest}$	n
Axolotl semicircular canal cells	439 ± 32 MΩ	17.7 ± 0.5 pF	-49 ± 1.4 mV	50
Axolotl utricle cells	331 ± 32 MΩ	12.1 ± 0.5 pF	-54 ± 1.2 mV	50

Ionic currents. The total ionic current was studied using seven cells from the semicircular canals and seven cells from the utricle. The most conspicuous difference between the semicircular canal and the utricle hair cell ionic currents was that the utricle cells have a much slower kinetics (Figure 4). The data obtained in Section 3 (see e) and f)) are presented in graphic form (see Figures 5 and 6) and in Table II.

In order to determine the exponent of the activation parameter (m^r), we used simple, double, triple, and quadruple exponential fittings to adjust the data as described in Section 3. The present data (Table II) correspond to the calculations conducted for $r = 3$ (the semicircular canal hair cells) and $r = 1$ (the utricle hair cells).

It is worth noting that, due to a complex nature and, in some cases, nonlinear behavior of the total ionic current in the hair cells, simple models cannot adjust some of the experimental recordings, indicating that more detailed models should be developed. Since, in addition, the complex nonlinear phenomena were found in our experiments, more detailed models should be developed. To determine the current inactivation time constant, an exponential function was adjusted to the current decay for the case of $V_{\rm test1}$ (see Figure 4). The filter properties of the semicircular canal and of the utricle hair cells are different (see Figure 4). A single exponential did not produce a correct adjustment to the inactivation time course; therefore, we decided to use two-exponential functions to fit the inactivation of the current. The data we obtained are shown in Figures 5, D and 6, D. Both τ_{h1} and τ_{h2} did not display a very clear voltage dependence (Figures 5 and 6).

Voltage responses. Hair cells do not generate action potentials in response to current pulse injection. Their voltage response to the current injection is characterized by a quasilinear voltage change to hyperpolarizing currents and a nonlinear flat response to depolarizing currents, thereby indicating that the input resistance decreases with depolarization (Figure 7).

5. Mathematical model of the total current. This model is a simplified representation of the hair cell dynamics. To construct it, we have supposed that individual ionic currents composing the total current have the same activation dynamics and at least two inactivation dynamics. The evaluation of the data presented in

Table II. Hair cells of the semicircular canal and of the utricle

parameter name	semicircular canal	utricle
C_m	14.3 ± 1.23 pF	10.13 ± 1.8 pF
g_{L}	2.32 ± 0.48 nS	0.48 ± 0.24 nS
g_{T}	78.51 ± 17 nS	28.14 ± 3.4 nS
E_{T}	-87 ± 15 mV	-87 ± 15 mV
$\tau_{\mathrm{ac}}(V_0)$	0.5 ± 0.1 ms	2.5 ± 0.5 ms
$\tau_{\max}$	11.41 ± 2.56 ms	10.76 ± 0.16 ms
$\tau_{\min}$	0.38 ± 0.03 ms	2.49 ± 0.34 ms
V_τ	-68.47 ± 7.35 mV	-41.23 ± 7.99 mV
S_τ	14.95 ± 2.72 mV	5.97 ± 1 mV
for variable activ. m.		
V_{ac}	-47.6 ± 7.3 mV	-16.32 ± 4 mV
S_{ac}	15.2 ± 2.5 mV	10.02 ± 2.43 mV
$m_{\min}$	0.25 ± 0.13	0.22 ± 0.04
for curved activ.		
$V_{\mathrm{cur-ac}}$	-25 ± 2 mV	-16.32 ± 4 mV
$S_{\mathrm{cur-ac}}$	17 ± 2 mV	10.02 ± 2.43 mV
$\min_{\mathrm{ac}}$	0.04 ± 0.03	0.22 ± 0.04
k_{h1}	-0.04 ± 0.05 ms/mV	0.27 ± 0.01 ms/mV
k_{h2}	0.14 ± 0.28 ms/mV	-0.57 ± 0.01 ms/mV
b_{h1}	45.08 ± 15.84 ms	32.02 ± 0.1 ms
b_{h2}	129.49 ± 22.25 ms	272.11 ± 0.1 ms
V_h	-65.23 ± 2.42 mV	-61.57 ± 1.57 mV
S_h	7.26 ± 1.28 mV	15.18 ± 1.34 mV
$h_{\min}$	0.38 ± 0.06	0.37 ± 0.01

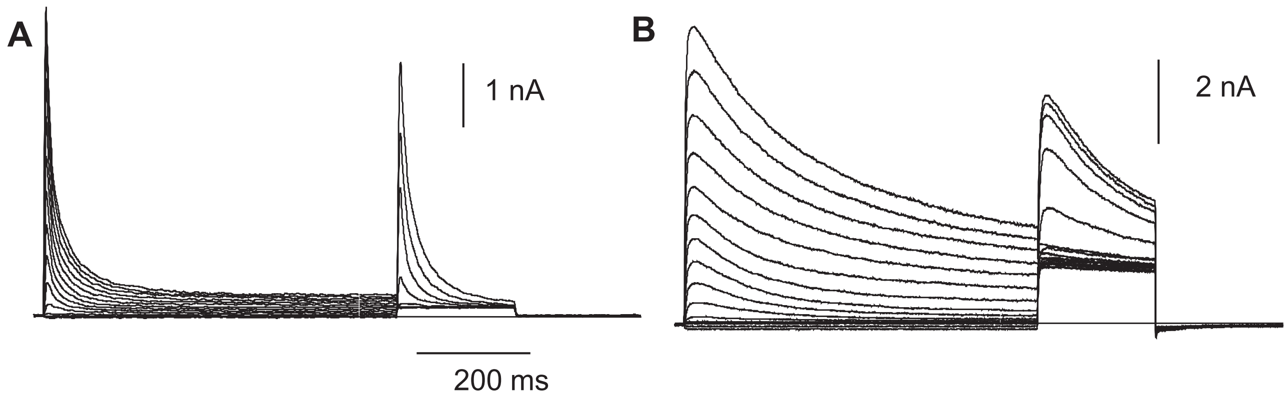

Fig. 4. The total ionic currents induced by the double-pulse voltage clamp protocol.
A: a cell from the semicircular canal. B: a cell from the utricle. The activation and inactivation kinetics of the ionic currents from the utricle cells are much slower than that from the semicircular canal cells. The value of τ_m for A at 0 mV was 1 ms and for B was 2.5 ms. The value of τ_h at 0 mV for A was adjusted with a double exponential with $\tau_{h1} = 11$ ms and $\tau_{h2} = 65$ ms and for B with $\tau_{h1} = 66$ ms and $\tau_{h2} = 291$ ms

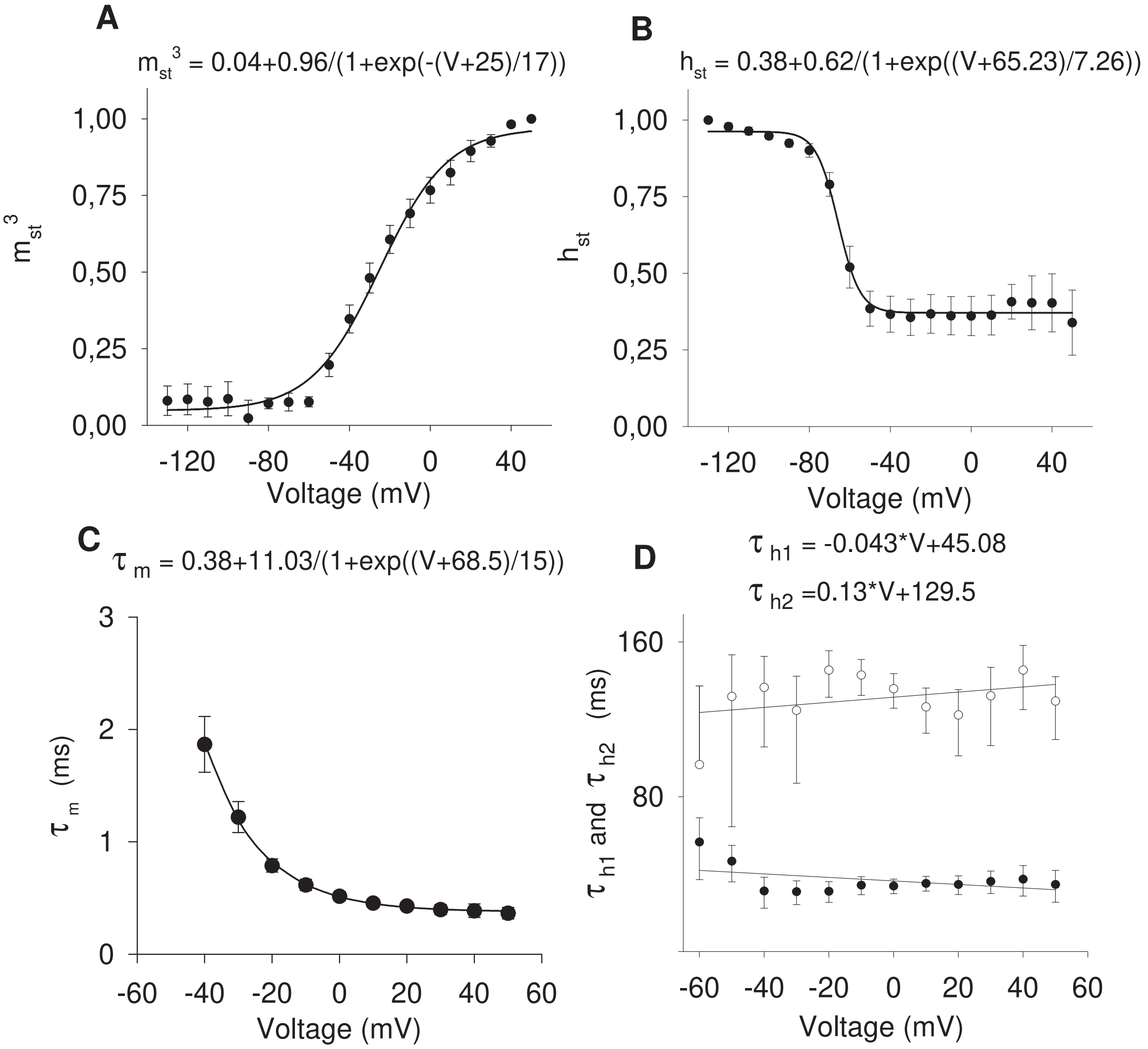

Fig. 5. Properties of the total current in the semicircular canal hair cells.
A and B: the curves of the activation (m^r) and inactivation (h) of the current as functions of voltage.
C: plot of τ_m versus voltage. Since the values of τ_m showed an extreme variability for V_{test1} less than -40 mV, they were not plotted. τ_m depends exponentially on the voltage. These values were approximated by a Boltzmann function. D: plots of τ_{h1} and τ_{h2} as functions of voltage were fitted with straight lines, thus indicating that the inactivation time constant had not a clear voltage dependence. Symbols represent the mean $\pm$ standard error $(n = 7)$

the experimental results allowed us to propose the following model:

$$
\begin{aligned}
&C_m \frac{dV}{dt} + I_{\mathrm{T}} + I_{\mathrm{L}} = I_{\mathrm{com}}, \quad I_{\mathrm{L}} = g_{\mathrm{L}} \cdot V, \quad I_{\mathrm{T}} = g_{\mathrm{T}} \cdot m^r \cdot (h_1 + h_2) \cdot (V - E_{\mathrm{T}}) \\
&\tau_m(V)\, \frac{dm}{dt} + m = m_{\mathrm{st}}(V) \\
&\tau_{h1}(V)\, \frac{dh_1}{dt} + h_1 = q_1 h_{\mathrm{st}}(V) = h_{1\mathrm{st}}(V) \\
&\tau_{h2}(V)\, \frac{dh_2}{dt} + h_2 = q_2 h_{\mathrm{st}}(V) = h_{2\mathrm{st}}(V)
\end{aligned}
\tag{23}
$$

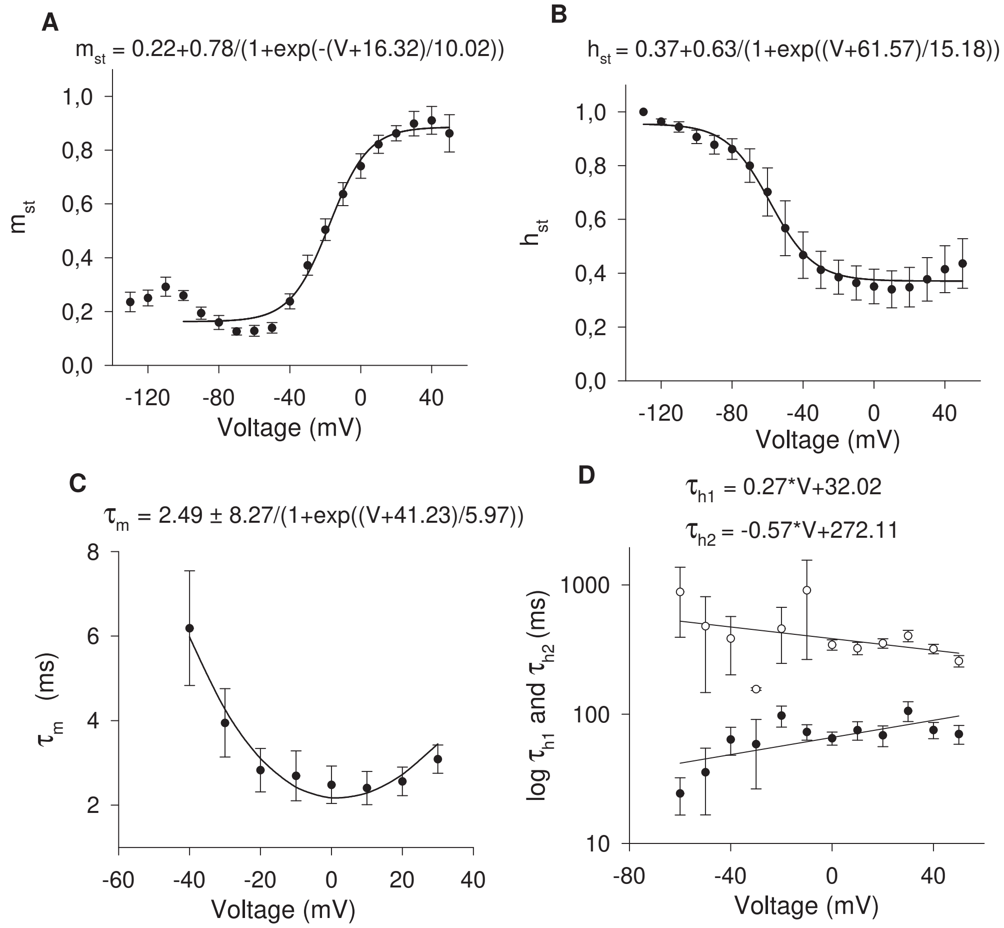

Fig. 6. Properties of the total current in the utricular hair cells. A and B: the curves for the activation (m^r) and inactivation (h) of the current as functions of voltage. C: plot of the activation time constant (τ_m) versus voltage. The data were adjusted with a first-order Boltzmann function for voltages ranging from -40 to $+30$ mV. The complex voltage dependence of τ_m for other voltages is probably due to the fact that some cells present a negative slope in the current-voltage curve for potentials above 20 mV. D: plots of the fast (τ_{h1}) and slow (τ_{h2}) inactivation time constants as functions of voltage. Both were adjusted using a linear fit. In all the graphs, each symbol represents the mean $\pm$ standard error $(n = 7)$

In the case of a natural stimulus the command current $I_{\rm com}$ corresponds to the transducer current $I_{\rm tr}$. In addition, we have

$$\begin{aligned}
&\tau_m(V) = \tau_{\min} + \frac{\tau_{\max} - \tau_{\min}}{1 + \exp\left(\frac{V - V_\tau}{S_\tau}\right)} \\
&m_{\rm st}(V) = m_{\min} + \frac{1 - m_{\min}}{1 + \exp\frac{-(V - V_{\rm ac})}{S_{\rm ac}}} \\
&h_{\rm st}(V) = h_{\min} + \frac{1 - h_{\min}}{1 + \exp\frac{V - V_h}{S_h}} \\
&\tau_{h1}(V) = k_{h1} \cdot V + b_1, \quad \tau_{h2}(V) = k_{h2} \cdot V + b_2
\end{aligned} \tag{24}$$

The numerical parameters of the above model were obtained from experimental results. We also used the values from Table II.

The mathematical model and the correctness of parameter values can be validated by the comparison

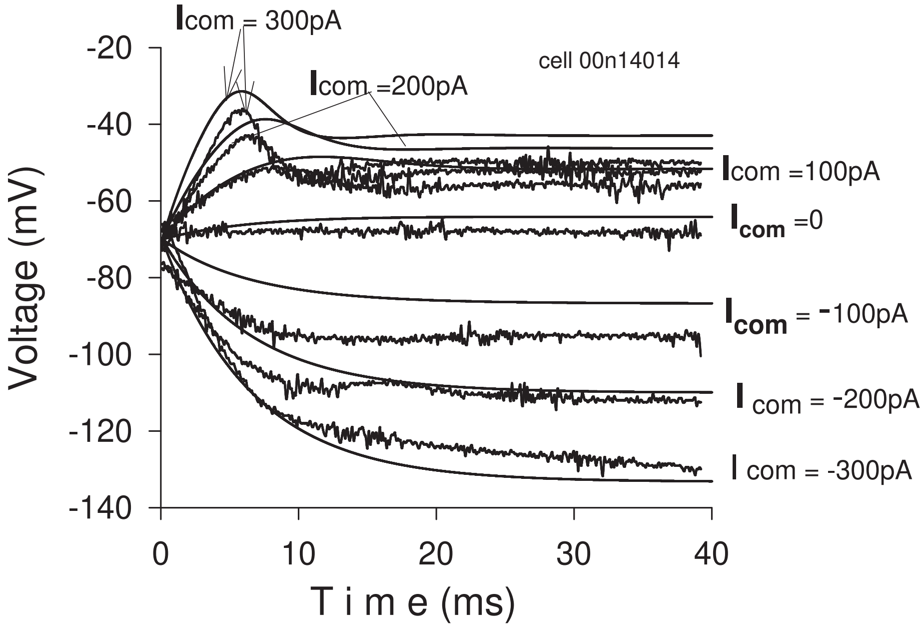

Fig. 7. Comparison of the experimentally measured response to current pulses from -300 to 300 pA (in steps of 100 pA) in a semicircular canal hair cell (00N14014) with the model voltage response trajectories. The thin (no noise) curves correspond to the model results. Parameter values in the model were chosen to produce accurate fits of the current response in the voltage clamp for the cell being studied. The model parameters were: $C_m = 15$ pF, $g_{\rm L} = 1.5$ nS, $g_{\rm T} = 79$ nS, $E_{\rm T} = -105$ mV, $h_{\min} = 0.115$, $V_h = -53.1$ mV, $S_h = 12.1$ mV, $r = 3$, $m_{\min} = 0.164$, $V_{\rm ac} = -29$ mV, $S_{\rm ac} = 9.09$ mV, $\tau_{\rm ac} = 0.396 + 93.77/(1+\exp((V+86.34)/14.24))$ ms, $\tau_{h1} = -0.233 \cdot V + 11.54$ ms, $\tau_{h2} = -0.778 \cdot V + 213.9$ ms. The model predicted a resting potential of -67 mV as well as a damped potential oscillation in response to depolarizing current pulses followed by a slowly developing depolarization and a passive response to hyperpolarizing stimulus

of model results with experimental data, using the current clamp protocol for certain cell types. We have used a computer program to obtain the current clamp protocol for the influences $I_{\rm com} = -300$ pA, -200 pA, -100 pA, 0 pA, 100 pA, 200 pA, and 300 pA. The general properties of voltage responses to the pulsed current in type II hair cells are: a passive response to a hyperpolarizing stimulus and a damped oscillatory response to a depolarizing stimulus.

Figure 7 compares the current clamp experimental results with our model results. The mathematical model satisfactorily reproduces the voltage response of hair cells to the current injection.

The model permits us to investigate the changes in the hair cell receptor potential not only under ordinary (usual) conditions, but in nontypical situations. For example, the phase tracks were constructed on the plane $(x = V, y = m)$ (see Figure 8). These tracks were obtained for different initial conditions taken for system (23) when $I_{\rm com} = 0$:

a) $V_0 = -10$ mV, $m = 0.3$, $h_1 = 1$, $h_2 = 0.1$;

b) $V_0 = -20$ mV, $m = 0.3$, $h_1 = 0.75$, $h_2 = 0.2$;

c) $V_0 = -30$ mV, $m = 0.53$, $h_1 = 0.5$, $h_2 = 0.3$;

d) $V_0 = -40$ mV, $m = 0.73$, $h_1 = 0.25$, $h_2 = 0.4$.

The numerical data taken from Table II for system (23) correspond to mean values of the parameters for the utricle hair cells. It is evident that all the tracks tend to the common equilibrium: $V = -75$ mV, $m_{\rm st} = 0.197$, $h_{1\rm st} = 0.81$, and $h_{2\rm st} = 0.81$.

6. Discussion. The model assumptions and simplifications are necessary for solving the problem of hair cell response. If in the above model we take into account all the ionic currents and every detail of hair cell electrical properties, then it would become as complex as the real thing; this inevitably makes the model extremely difficult to deal with and unfeasible to incorporate as a part of a global model of the vestibular system.

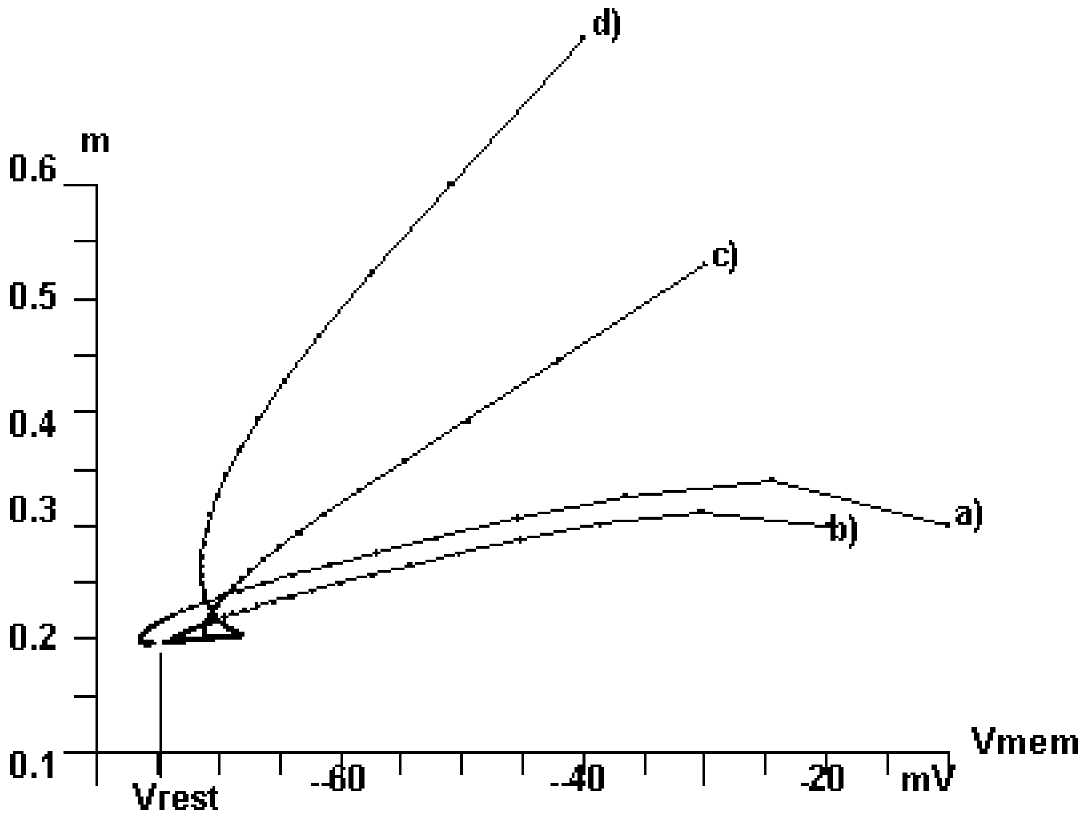

Fig. 8. The phase tracks were constructed on the plane ($x = V, y = m$). These tracks were obtained for different initial conditions taken for system (23): a) $V_0 = -10$ mV, $m = 0.3$, $h_1 = 1$, $h_2 = 0.1$; b) $V_0 = -20$ mV, $m = 0.3$, $h_1 = 0.75$, $h_2 = 0.2$; c) $V_0 = -30$ mV, $m = 0.53$, $h_1 = 0.5$, $h_2 = 0.3$; d) $V_0 = -40$ mV, $m = 0.73$, $h_1 = 0.25$, $h_2 = 0.4$. The numerical data taken from Table II for system (23) correspond to mean values of the parameters for the utricle hair cells. It is evident that all the tracks tend to the common equilibrium: $V_{\rm rest} = -75$ mV, $m_{\rm st} = 0.197$, $h_{1\rm st} = 0.81$, and $h_{2\rm st} = 0.81$

There are several assumptions implicit for the model presented here: 1) the ionic currents can be regarded as a single total ionic current with only one activation and two inactivation processes; 2) the voltage-sensitive permeabilities for K^+ ions are absolutely dominant and located in the basolateral membrane; 3) the only input to the hair cells is the transducer current (no other inward currents, like the currents induced by the efferent synapses or the modulatory influences, are taken into account).

The passive properties of the axolotl hair cells are well within the range described for the type II hair cells (see Table III). The only parameter for which we have found an extreme value is the membrane capacitance in the semicircular canals.

Table III. Passive properties of hair cells in various systems

	Animal	R_m	C_m	$V_{\rm rest}$	n
Axolotl semicircular canal cells	Axolotl	439 ± 32 MΩ	17.7 ± 0.5 pF	-49 ± 1.4 mV	50
Axolotl utricle cells	Axolotl	331 ± 32 MΩ	12.1 ± 0.5 pF	-54 ± 1.2 mV	50
Rennie and Ashmore, 1991	Guinea pig	-	5.3 ± 1.6 pF	-48 ± 11 mV	10
Ricci et al., 1994	Frog	386 ± 151 MΩ	10.4 ± 0.7 pF	-45 ± 1 mV	154
Masetto et al., 1994	Frog periphery	1.5 ± 0.15 GΩ	9.16 ± 0.36 pF	-46 ± 1.3 mV	27
Masetto et al., 1994	Frog central area	1.14 ± 0.1 GΩ	12.3 ± 0.52 pF	-58 ± 1.8 mV	18

In contrast, the type I hair cells (see Table IV) have completely different passive properties indicating that their membrane characteristics are significantly different from those of the type II hair cells.

Table IV. Passive properties of type I hair cells

	Animal	Resistance	Capacitance	V_{rest}	n
Rennie et al., 1996	Gerbil	21.4 ± 14 MΩ	3.4 ± 1.7 pF	-67 ± 9 mV	25
Rennie et al., 1991	Guinea pig		4.5 ± 1.2 pF	-48 ± 10 mV	35

The ionic currents found in the hair cells of the axolotl also coincide in general with those found in other biological preparations, such as the frog, the pigeon, and the guinea pig [3, 4, 6, 15, 17, 18, 20, 22, 24]. In comparison with other types of excitable cells (in particular, neurons), the hair cells lack the fast inward Na^+ current. Therefore, a depolarizing stimulus, such as the activation of the transducer current, produces a cell response that is based on the activation of the K^+ outward and Ca^{2+} inward currents. The Ca^{2+} currents in the axolotl hair cells as well as those described for other species [23] are very small in comparison with the K^+ currents ([31]; Vega et al, in this book). As a consequence, the outward K^+ currents mainly dominate the response of the hair cells and the Ca^{2+} currents are indistinguishable unless the K^+ currents are blocked. This is the reason why the effect of a current pulse is very similar to a passive response with a decay in the membrane resistance upon depolarization.

From this and previous works, it is clear that the outward K^+ currents in the hair cells are of various types, including the inactivating and noninactivating currents. It seems that the differential expression of activating and noninactivating currents will produce a gradation of responses of the hair cells, forming a continuum from the cells that predominantly express the inactivating currents to those that mainly express the noninactivating currents. However, the functional significance of the inactivating and noninactivating currents in shaping the hair cells responses is not completely clear. This is one of the reasons for the need to develop hair cell models which ensure the full understanding of the influence of different current amplitudes and kinetics on cell response shapes.

It is worth noting that we have found no clear correlation between the morphology of the hair cells (round, cylindrical, club-like, etc.) and its ionic currents. Instead, we found a significant correlation between the hair cell endorgan source and the ionic current kinetics. The semicircular canal cells possess a much faster kinetics than those from the utricle. Preliminary results obtained at our laboratory suggest that the saccular hair cells have a slow kinetics similar to that of the utricular cells. Another significant difference we are actually investigating is that the hair cells from the utricle express a bigger inward rectifier current than the semicircular canal cells.

In current clamp recordings of hair cells of both the utricle and the semicircular canals, we found no clear evidence of electrical resonance except for a very damped oscillation in both cell types. When analyzing current clamp responses, possible artifactual oscillations derived from the clamp amplifier should be taken into account [21]. So, the faint oscillations we have observed cannot conclusively be thought of as having a cellular origin. The strong differences in the ionic currents kinetics between utricular and semicircular canal hair cells lead to significant differences in their voltage responses to the current pulse injection. The semicircular canal cells show a fast damping response. In comparison, the utricular hair cells have a bigger initial slowly damping voltage response. The significance of these differences in the voltage response for the physiology of hair cells can be accurately resolved by mathematical modeling.

A similar attempt to model the whole vestibular system of an endorgan has been carried out by Segal and Outerbridge [28]. These authors presented a model of responses of the semicircular canals, using a system of nonlinear third-order ordinary differential equations with eight parameters. However, the hair cells in this model appear as linear elements and no attention at all is given to their response. Other modeling attempts have been mainly directed to explain the oscillatory responses found in hair cells of the frog sacculus [5, 14, 17, 18]. The work presented here constitutes one of the first approaches to the problem of simulating the hair cell dynamics, using the Hodgkin–Huxley type models with an accurate definition of model parameters in a biological system.

The simplified model we proposed allows simulating the hair cell response dynamics and constitutes a research tool on the basis of which an in-depth analysis of hair cell responses can be developed. Note that our model is a simplified one and constitutes a first approach to the problem of hair cell modeling. This simplified model is ideally suited for the incorporation into a general model of vestibular system dynamics, as stated in the introduction to this paper.

7. Acknowledgments. This research was partially supported by the CONACyT grant 35525-N to E.S. and by the CONACyT fellowships 137444 to AA and 124156 to AL.

REFERENCES

1. C.M. Armstrong and W.F. Gilly, "Access resistance and space clamp problems associated with whole-cell patch clamping", *Meth. Enzimol.*, 207: 100–122, 1992.
2. Axon Instruments web site, http://www.axon.com
3. M.J. Correia and D.G. Lang, "An electrophysiological comparison of solitary type I and type II vestibular hair cells", *Neurosci. Lett.*, 116: 106–111, 1990.
4. M.J. Correia, "Filtering properties of hair cells", *Ann. NY Acad. Sci.*, 656: 182–203, 1992.
5. A.C. Crawford and R. Fettiplace, "An electrical tuning mechanism in turtle cochlear hair cells", *J. Physiol.*, 312: 377-412, 1981.
6. R.A. Eatock and M.J. Hutzler, "Ionic currents of mammalian vestibular hair cells", *Ann. NY Acad. Sci.*, 656: 58–74, 1992.
7. R.A. Eatock and A. Rüsch, "Developmental changes in the physiology of hair cells", *Cell Develop. Biol.*, 8: 265–275, 1997.
8. B. Frankenhaeuser, "Quantitative description of sodium currents in myelinated nerve fibres of *Xenopus laevis*", *J. Physiol.*, 151: 491–501, 1960.
9. O.P. Hamill, A. Marty, E. Neher, B. Sakman, and S.J. Sigworth, "Improved patch clamp technique for high resolution current recording from cell and cell free membrane patches", *Pflügers Arch.*, 391: 85-100, 1981.
10. A.L. Hodgkin and A.F. Huxley, "Currents carried by sodium and potassium ions through the membrane of the giant axon of Loligo", *J. Physiol.*, 116: 449–472, 1952.
11. A.L. Hodgkin and A.F. Huxley, "The components of membrane conductance in the giant axon of Loligo", *J. Physiol.*, 116: 473–496, 1952.
12. A.L. Hodgkin and A.F. Huxley, "The dual effect of membrane potential on sodium conductance in the giant axon of Loligo", *J. Physiol.*, 116: 497–506, 1952.
13. A.L. Hodgkin and A.F. Huxley, "A quantitative description of membrane current and its application to conduction and excitation in nerve", *J. Physiol.*, 117: 500–544, 1952.
14. J.R. Holt and R.A. Eatock, "Inwardly rectifying currents in succular hair cells from the leopard frog", *J. Neurophysiology*, 73: 1484–1502, 1995.
15. G.D. Housley, C.H. Norris, and P.S. Guth, "Electrophysiological properties of hair cells isolated from the semicircular canal of the frog", *Hearing Research*, 38: 259–276, 1989.
16. A.J. Hudspeth, "The ionic channels of a vertebrate hair cell", *Hearing Research*, 22: 21–27, 1986.
17. A.J. Hudspet and R.S. Lewis, "Kinetic analysis of voltage- and ion-dependent conductances in saccular hair cells of the bullfrog", *J. Physiol.*, 400: 237–47, 1988.
18. A.J. Hudspeth and R.S. Lewis, "A model for electrical resonance and frequency tuning in saccular hair cells of the bullfrog", *J. Physiol.*, 400: 275–297, 1988.
19. V.S. Markin and A.J. Hudspeth, "Gating-spring models of mechanoelectrical transduction by hair cells of the internal ear", *Annu. Rev. Biophys. Biomol. Struct.*, 24: 59–83, 1995.
20. S. Masetto, G. Russo, and I. Prigioni, "Differential expression of potassium currents by hair cells in thin slices of frog crista ampullaris", *J. Neurophysiol.*, 72: 443–455, 1994.
21. S. Masetto, T. Weng, P. Valli, and M.J. Correia, "Artifactual voltage response recorded from hair cells with patch clamp amplifiers", *NeuroReport*, 10: 1837–1841, 1999.
22. C.H. Norris, A.I. Ricci, G.D. Housley, and P.S. Guth, "The inactivating potassium currents of hair cells isolated from the crista ampullaris of the frog", *J. Neurophysiol.*, **68**, 5, 1992.
23. I. Prigioni, S. Masetto, G. Russo, and V. Taglietti, "Calcium currents in solitary hair cells isolated from frog crista ampullaris", *J. Vest. Res.*, 2: 31-39, 1992.
24. K.J. Rennie and J.F. Ashmore, "Ionic currents in isolated vestibular hair cells from the guinea-pig crista ampullaris", *Hearing Research*, 51: 279–292, 1991.

25. K.J. Rennie, A.J. Ricci, and M.J. Correia, "Electrical filtering in gerbil isolated type I semicircular canal hair cells", *J. Neurophysiol.*, 75: 2117–2123, 1996.

26. A.J. Ricci, C. Erostegui, R.P. Bobbin, and C.H. Norris, "Comparative electrophysiological properties of guinea pig (*Cavia cobaya*) outer hair cells and frog (*Rana pipiens*) semicircular canal hair cells", *Comp. Biochem. Physiol.*, **107A**, 1: 13–21, 1994.

27. A.J. Ricci, and R. Fettiplace, "Calcium permeation of the turtle hair cell mechanotransducer channel and its relation to the composition of endolymph", *J. Physiol.*, 506: 159-173, 1998.

28. B.N. Segal and J.S. Outerbridge, "A nonlinear model of semicircular canal primary afferents in bullfrog", *J. Neurophysiol.*, 47: 563–578, 1982.

29. E. Soto and R. Vega, "Actions of excitatory amino acid agonists and antagonists on the primary afferents of the vestibular system of the axolotl (*Ambystoma mexicanum*)", *Brain Res.*, 462: 104–111, 1988.

30. E. Soto, A. Flores, C. Erostegui, and R. Vega, "Evidence for NMDA receptor in the afferent synaptic transmission of the vestibular system", *Brain Res.*, 633: 289–29, 1994.

31. R. Vega, *Papel fisiológico y mecanismo de acción de neuropéptidos en el oído interno*, Tesis de Doctorado, Instituto de Investigaciones Biomédicas, Universidad Nacional Autónoma de México, 2001.

32. R. Vega, R. Budelli, and E. Soto, "The receptor potential–synaptic transmission problem in type I hair cells", *Abs. Assoc. Res. Otolaryngol.*, 23: 580, 2000.